

Beyond Words: Enhancing Desire, Emotion, and Sentiment Recognition with Non-Verbal Cues

Wei Chen^{a,b,c,d}, Tongguan Wang^{a,b,c,d}, Feiyue Xue^{a,b,c,d}, Junkai Li^{a,b,c,d}, Hui Liu^{a,b,c,d}, Ying Sha^{a,b,c,d,*}

^aKey Laboratory of Smart Farming for Agricultural Animals, No.1 Shizishan Street, Hongshan District, Wuhan, 430070, Hubei, China

^bEngineering Research Center of Intelligent Technology for Agriculture, Ministry of Education, No.1 Shizishan Street, Hongshan District, Wuhan, 430070, Hubei, China

^cHubei Engineering Technology Research Center of Agricultural BigData, No.1 Shizishan Street, Hongshan District, Wuhan, 430070, Hubei, China

^dCollege of Informatics, Huazhong Agricultural University, No.1 Shizishan Street, Hongshan District, Wuhan, 430070, Hubei, China

Abstract

Desire, as an intention that drives human behavior, is closely related to both emotion and sentiment. Multimodal learning has advanced sentiment and emotion recognition, but multimodal approaches specially targeting human desire understanding remain underexplored. And existing methods in sentiment analysis predominantly emphasize verbal cues and overlook images as complementary non-verbal cues. To address these gaps, we propose a Symmetrical Bidirectional Multimodal Learning Framework for Desire, Emotion, and Sentiment Recognition, which enforces mutual guidance between text and image modalities to effectively capture intention-related representations in the image. Specifically, low-resolution images are used to obtain global visual representations for cross-modal alignment, while high resolution images are partitioned into sub-images and modeled with masked image modeling to enhance the ability to capture fine-grained local features. A text-guided image decoder and an image-guided text decoder are introduced to facilitate deep cross-modal interaction at both local and global representations of image information. Additionally, to balance perceptual gains with computation cost, a mixed-scale image strategy is adopted, where high-resolution images are cropped into sub-images for masked modeling. The proposed approach is evaluated on MSED, a multimodal dataset that includes a desire understanding benchmark, as well as emotion and sentiment recognition. Experimental results indicate consistent improvements over other state-of-the-art methods, validating the effectiveness of our proposed method. Specifically, our method outperforms existing approaches, achieving F1-score improvements of 1.1% in desire understanding, 0.6% in emotion recognition, and 0.9% in sentiment analysis. Our code is available at: <https://github.com/especiallyW/SyDES>.

Keywords: Human Desire Understanding, Sentiment Analysis, Emotion Recognition, Multimodal Learning, Multimodal Fusion

1. Introduction

Social media platforms such as Twitter and Instagram have become widely used channels for sharing personal experiences and opinions. On these platforms, users post multimodal content including images, text, and audio, making emotion expression and sentiment analysis important topics in natural language processing and computational social science. Over the past decades, research has progressed from text-only emotion and sentiment analysis [1, 2, 3] to multimodal approaches [4, 5, 6], which have shown wide applicability in dialogue understanding, public opinion monitoring, and human-computer interaction. However, the specific problem of desire understanding, which an underlying driver of human emotion, has received comparatively little dedicated attention.

Desire is a fundamental human intention that reflects a strong wish for certain objects or states, and it constitutes one of the traits distinguishing humans from other animals [7]. Desire interacts closely with emotion and sentiment. It can shape affective life experiences, and conversely, sentiment and emotional

states may modulate the expression or strength of desire. Such three tasks form interconnected and essential components of the human experience, driving our actions and decisions. For example, in Figure 1 (a), a couple smiling and preparing food in a kitchen can be interpreted as expressing a "romance" desire, which explains positive sentiment and happy emotion. Figure 1 (b) depicts a man's exaggerated movements to avoid security cameras. It can be understood as fear and negative sentiment driven by a desire for safety and privacy. Therefore, if a machine were capable of accurately inferring such desire intents, it would move research closer to recognizing human emotional intelligence [8].

With the rapid development of multimodal learning and the prevalence of social media data, multimodal sentiment analysis and emotion recognition have attracted increasing attention. However, most existing methods still concentrate on enhancing and modeling verbal cues (e.g., via graph neural networks), such as [9, 10], while image-based non-verbal cues are often treated only as features to be extracted and fused superficially. In practice, non-verbal cues play a crucial role. For example, the grimacing expression in Figure 1 (c) could indicate disgust toward broccoli or be part of a playful interaction with family;

*Corresponding author.

Email address: shaying@mail.hzau.edu.cn (Ying Sha)

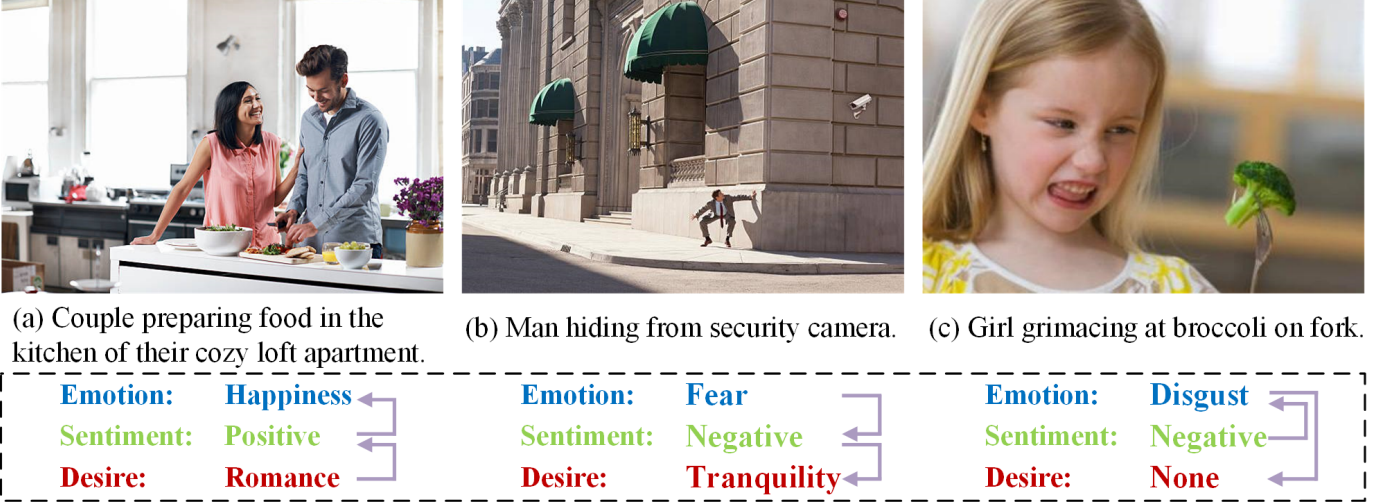


Figure 1: Examples of multimodal desire, emotion, and sentiment.

without image context, text-based inference may be ambiguous. Whereas incorporating image information can lead to a correct interpretation of the emotion, such as disgust.

Motivated by these observations, we propose SyDES, a *Symmetrical Bidirectional Multimodal Learning Framework for Desire, Emotion, and Sentiment recognition*. The framework emphasizes deep utilization of non-verbal visual cues while ensuring that verbal cues remain effectively exploited. Specifically, the input image is processed as both a low-resolution version and a high-resolution version using a shared image encoder. The low-resolution image provides global visual representations for cross-modal alignment. The high-resolution image is processed by mixed-scale image strategy to get high-resolution sub-images, and these sub-images are modeled with masked image modeling to encourage the encoder to better learn fine-grained local features. A text-guided image decoder is introduced so that image reconstruction can be guided by textual semantics. Conversely, an image-guided text decoder is employed so that text decoding can incorporate multi-scale visual information. In the meantime, we design a set of loss functions (e.g., local-global semantic similarity loss, cross-modal feature-distribution consistency loss) to allow reconstructed image to maintain modal alignment of fine-grained local visual features and global visual representations, thereby avoid over-reliance on specific regional features. These mechanisms enable mutual guidance and semantic alignment of textual representations, local visual features and global visual features. The fused text outputs are then passed to a lightweight multi-layer perception (MLP) for downstream prediction (see Figure 2 and Section 3 for details).

To evaluate our approach, extensive experiments are conducted on MSED dataset, the first multimodal dataset that includes benchmarks for desire understanding, emotion recognition, and sentiment analysis. In addition to desire task, evaluations are performed on the emotion and sentiment recognition. Results show that our proposed SyDES outperforms existing methods across all three tasks, with F1-score improve-

ments of approximately 0.9% for sentiment analysis, 0.6% for emotion recognition, and 1.1% for desire understanding. These findings demonstrate the effectiveness of a vision-driven modal guidance strategy for intensive representation and generalization. Our contributions can be summarized:

- (1) We introduce SyDES, a symmetrical bidirectional multimodal learning framework that enhances the utilization of non-verbal cues while preserving the effectiveness of textual signals, thereby improving desire understanding, emotion recognition, and sentiment analysis.
- (2) To reconcile the differing objectives of modal alignment and masked image modeling, we design a set of loss functions that balance these objectives, enabling the model to learn fine-grained visual features while maintain semantic-level modal consistency.
- (3) We provide comprehensive experiments and ablation studies on the MSED dataset, validating the effectiveness and generalization of our proposed SyDES for multimodal desire understanding, emotion recognition, and sentiment analysis.

2. Related Work

2.1. Sentiment Analysis and Emotion Recognition

2.1.1. Text-only sentiment analysis

Sentiment analysis [1, 11, 12, 13] has long been a central research topic in NLP. Early researches often operated in a unimodal setting. For example, Taboada et al. [14] proposed a lexicon-based method called the Semantic Orientation CALculator, which uses a lexicon annotated with semantic orientation and incorporates negation handling to determine polarity. Pang et al. [11] and Gamallo et al. [15] applied classical machine learning techniques for text sentiment classification, including support vector machine (SVM) and Naïve Bayes. Kim et al. [1] was among the first to apply convolutional neural networks

to text classification. Tai et al. [12] considered syntactic structures of natural language and proposed the tree-structured long short-term memory (Tree-LSTM) to model hierarchical dependencies. Yang et al. [2] designed a Hierarchical Attention Network (HAN) for document-level sentiment classification, which introduces the attention mechanism to assist networks in selecting important words and sentences. Similarly, Wang et al. [16] integrated attention into LSTM to strengthen aspect-level sentiment associations within sentences. More recently, Singh et al. [13] applied BERT to sentiment analysis on COVID-related tweets. These approaches predominantly rely on unimodal signals. In real-world social media scenarios, however, text is often accompanied by images; relying solely on text is therefore insufficient because multimodal cues typically provide complementary information to facilitate more accurate prediction.

2.1.2. Multimodal sentiment analysis and emotion recognition

Multimodal sentiment classification [17, 18, 19] has attracted increasing attention as researchers seek to jointly analyze sentiment from multiple modalities. You et al. [17] introduced cross-modal consistency regression (CCR) to jointly classify sentiment using image and text features. Xu et al. [4] leveraged scene-level visual cues and attention mechanisms to identify important words and sentences. Hu et al. [20] focused on user’s latent emotion states. From a modality-interaction perspective, Xu et al. [18] explored iterative relations between image and text. Huang et al. [19] used hybrid fusion strategies to enable between unimodal and cross-modal representations. Li et al. [21] applied contrastive learning and data augmentation to align and fuse the token-level features of text and image. Meanwhile, multimodal emotion recognition [22, 23, 24], which targets finer-gained affective states than coarse sentiment, has also been widely studied. To capture reader’s emotional reactions to new articles, Guo et al. [25] introduced two multimodal news datasets and proposed a layout-driven network. Nemaïti et al. [26] proposed a hybrid method for latent-space data fusion. Zhang et al. [23] used manifold learning and deep convolutional networks to extract low-dimensional emotion-relevant features. Xu et al. [27] adopted image captions as semantic cues for multimodal prediction. Yang et al. [5] updated image-text features within a memory network and introduced a multi-view attention network for multimodal integration. Despite these advances, most of the existing approaches simply leveraged holistic or local features extracted from different modalities to predict multimodal sentiments, which leads to suboptimal performance.

The emergence of graph neural networks (GNNs) [28, 29] has opened new directions for mining relationships among verbal cues. Yang et al. [9] observed that emotional expression exhibits specific global features and introduced a multi-channel GNN to model global attributes, aiming to mine commonalities in language signals. Similarly, Zhang et al. [30] proposed a multi-task interactive graph-attention network with local-global context connection module to model contextual relationships. Wang et al. [31] enriched textual representations by leveraging contextual world knowledge from large multimodal models. However, these approaches predominantly focus on mining ver-

bal cues and often underutilize the rich information contained in non-verbal cues.

Motivated by the importance of non-verbal cues, we hope to attain fine-grained features from image contextual information. Masked image modeling paradigm introduced by He et al. [32] has shown that an encoder can be encouraged, via a reconstruction-based self-supervised objective, to learn richer local representations. This insight motivates our proposal of a symmetrical bidirectional multimodal learning framework to ensure more effective exploitation of image-based non-verbal cues for desire understanding, emotion recognition, and sentiment analysis.

2.2. Multimodal Desire Understanding

Multimodal desire understanding concerns recognizing desires or intentions expressed in both textual and visual expression, and it remains an underexplored problem. Existing automated analyses of desire largely originate from psychology and philosophy. Lim et al. [33] developed a desire-understanding system based on four emotional states in audio and gestural cues. Cacioppo et al. [34] designed a multi-level kernel-density fMRI analysis to investigate differences and correlations between sexual desire and love. Schutte et al. [35] conducted a meta-analysis on 2,692 participants to examine links between curiosity and creativity. Hoppe et al. [36] estimated different levels of curiosity using eye-movement data and SVM. Yavuz et al. [37] proposed a data-mining approach for desire and intent using neural networks and Bayesian networks. Chauhan et al. [38] presented a multi-task multimodal deep attentive framework for offense, motivation, and sentiment analysis. Nevertheless, these researches commonly lack support for large-scale multimodal social media data and often do not fully exploit both visual and textual channels.

To address these limitations, Jia et al. [39] introduced MSED dataset, the first multimodal dataset for desire understanding. MSED collects image-text pairs from social media and defines three sub-tasks, including desire understanding, emotion recognition, and sentiment analysis. They also provide various strong baselines based on different combinations of feature representations using various image and text encoders. Aziz et al. [40] attempted to combine two multimodal models into a unified architecture (MMTF-DES) to achieve ensemble-like performance and reported improved results on desire understanding. However, this strategy increases training and inference cost. Motivated by the need to fully exploit image-based non-verbal cues while maintaining computational efficiency, we propose a symmetrical bidirectional multimodal learning framework, offering a new method for multimodal desire understanding.

3. SyDES

Figure 2 illustrates overall architecture of SyDES. In this section, we first introduce the mixed-scale image strategy and motivate its necessity. We then describe in detail each component of the architecture, including the image encoder, text encoder, text-guided image decoder, and image-guided text decoder. Next, we present the loss functions used during training

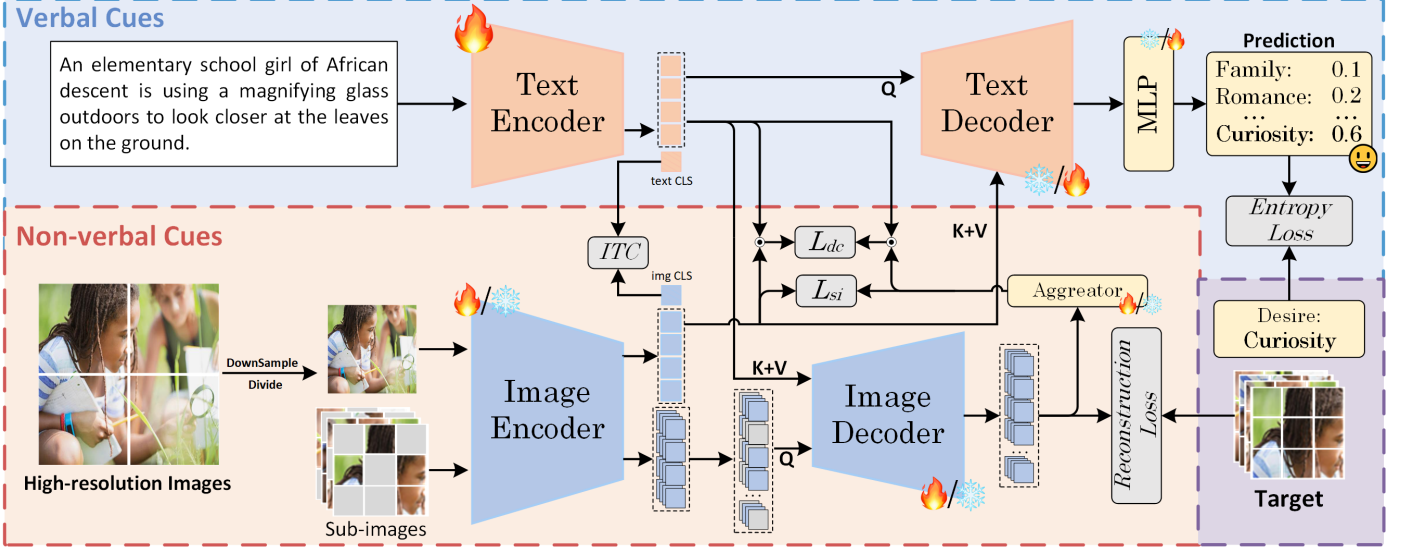


Figure 2: Overall architecture of SyDES. The model consists of four core modules: an image encoder, a text encoder, a text-guided image decoder, and an image-guided text decoder.

and explain how they support downstream performance. Finally, we discuss the two-stage training paradigm and its rationale.

3.1. Mixed-Scale Image Strategy

High-resolution images can capture richer region-level features and local details. However, many multimodal models conventionally operate on 224×224 images, which constrains their capacity for fine-grained visual perception. Directly increasing the encoder input resolution (e.g., processing all inputs at 448×448) dramatically increases computational cost.

To balance fine-grained feature extraction and computational efficiency, we adopt a mixed-scale sub-images strategy to get detailed high-resolution visual features. Given a high-resolution image I_i from batch size N , e.g., 448×448 , we produce one downsampled low-resolution image and four high-resolution sub-images, resulting in five 224×224 images per original image. This provides four sets of fine-grained local features and one global representation while controlling computational overhead. Formally:

$$\begin{aligned} I_i^{(1)} &= \text{DownSample}(I_i), & I_i^{(1)} &\in \mathbb{R}^{224 \times 224 \times 3} \\ I_i^{(2,n)} &= \text{Crop}_n(I_i), & I_i^{(2,n)} &\in \mathbb{R}^{224 \times 224 \times 3}, \quad n = 1, 2, 3, 4 \end{aligned} \quad (1)$$

where DownSample may use bilinear interpolation, and Crop_n denotes corner or predefined cropping. Each 224×224 image is treated as an independent input to the image encoder to obtain global and local representations.

3.2. Model Architecture

Our proposed SyDES comprises four modules: an image encoder, a text encoder, a text-guided image decoder, and an image-guided text decoder, together with a lightweight MLP for downstream prediction.

3.2.1. Image Encoder

We employ a vision transformer [41] as the image encoder in order to extract global representation from low-resolution images and capture local details from high-resolution sub-images. We attain $I_i^{(1)}$ and $I_i^{(2,n)}$ after the mixed-scale image strategy. Each 224×224 image is split into P patches and embedded as:

$$\begin{aligned} P_{\text{emb},i}^{(1)} &= [v_i^{\text{cls}}, v_i^1, \dots, v_i^P] \in \mathbb{R}^{(P+1) \times C_1} \\ P_{\text{emb},i}^{(2,n)} &= [v_{i,n}^{\text{cls}}, v_{i,n}^1, \dots, v_{i,n}^P] \in \mathbb{R}^{(P+1) \times C_1} \end{aligned}$$

where C_1 denotes the image embedding dimension and v_i^{cls} is the CLS token. For high-resolution sub-images $I_i^{(2,n)}$, we apply a binary mask vector $m_{i,n} \in \{0, 1\}^P$ with $m_{i,n}[P] = 1$ indicating that patch p is masked. Following the Masked Auto-Encoder (MAE) [32], we set the mask ratio to $m \in [0, 1]$ and set the keep ratio to $r = 1 - m$. The set of unmasked indices is $M_{i,n} = \{p \mid m_{i,n}[p] = 0\}$ with $|M_{i,n}| = rP$. Selecting the unmasked tokens yields:

$$\tilde{P}_{\text{emb},i}^{(2,n)} = \text{Select}(P_{\text{emb},i}^{(2,n)}, M_{i,n}) \in \mathbb{R}^{(rP+1) \times C_1}$$

Both $P_{\text{emb},i}^{(1)}$ and $\tilde{P}_{\text{emb},i}^{(2,n)}$ are fed into the shared image encoder to produce $V_i^{(1)} \in \mathbb{R}^{(P+1) \times C_1}$ and $V_i^{(2,n)} \in \mathbb{R}^{(rP+1) \times C_1}$, where the first row of $V_i^{(1)}$ corresponds to the low-resolution CLS visual feature $v_i^{\text{cls}} \in \mathbb{R}^{C_1}$.

3.2.2. Text Encoder

As the text encoder, we adopt a causal masked transformer encoder to model text inputs. Text inputs are tokenized by BPE into an embedding sequence of length S represented as $W_{\text{emb},i}$. The sequence is encoded by a causal masked transformer to avoid future information leakage and attain encoding features:

$$W_i = [w_i^1, \dots, w_i^{S-1}, w_i^{\text{cls}}] \in \mathbb{R}^{S \times C_2}$$

with $w_i^{\text{cls}} \in \mathbb{R}^{C_2}$ being the CLS text feature and C_2 denotes the text embedding dimension.

3.2.3. Text-guided Image Decoder

To recover masked patches from $\tilde{P}_{\text{emb},i}^{(2,n)}$ and make reconstruction aware of textual semantics, we adopt a text-guided image decoder. Specifically, we utilize cross-attention transformer modules to deeply fuse image and text information. We project $V_i^{(2,n)}$ to the text embedding dimension C_2 , and introduce mP shared and learnable mask tokens $P_{\text{mask}} \in \mathbb{R}^{mP \times C_2}$. The decoder input is:

$$D_{i,n}^{\text{in}} = [P_{\text{mask}}; \text{Proj}(V_i^{(2,n)})] \in \mathbb{R}^{(mP+rP+1) \times C_2}$$

To achieve stable modal fusion, a gate-based fusion mechanism is used to combine intermediate image projections and text features:

$$W_{i,n}^{\text{comb}} = \text{Gate}(W_i, D_{i,n}^{\text{in}}) \in \mathbb{R}^{(rP+mP+1) \times C_2}$$

As utilizing $D_{i,n}^{\text{in}}$ as the query and $W_{i,n}^{\text{comb}}$ as the key and value, we leverage textual semantic information to compel the masked image reconstruction process to perceive verbal cues, thereby facilitating the generation of reconstructed images with cross-modal characteristics. The image decoder predicts the pixel values of masked image patches and a sub-image-level global representation:

$$\{\tilde{X}_{i,n}^p\}_{p \in \bar{M}_{i,n}} = \text{ImgDec}(D_{i,n}^{\text{in}}, W_{i,n}^{\text{comb}}) \in \mathbb{R}^{(rP+mP+1) \times C_2}$$

where $\tilde{X}_{i,n}^p$ denotes the predicted pixel value for the p -th masked patch in the n -th sub-image of the i -th high-resolution image, $\bar{M}_{i,n}$ represents the set of masked indices in the n -th sub-image of the i -th high-resolution image, and ImgDec refers to the text-guided image decoder. Furthermore, the decoder outputs a set of sub-image-level global representation $z_{i,n} \in \mathbb{R}^{n \times C_2}$, which is used for subsequent aggregation and similarity loss calculation to better maintain modal alignment between fine-grained local features and global visual representations.

3.2.4. Image-guided Text Decoder

Similarity, to enable the text decoder to incorporate multi-scale visual cues, we adopt an image-guided text decoder. More specifically, we use non-CLS text tokens as the query, and the concatenation of $V_i^{(1)}$ and $V_i^{(2,n)}$ as the key and value. This enables the fusion of textual and multi-scale visual information from low-resolution images and high-resolution sub-images. Ultimately, we obtain a multimodal feature $\tilde{W}_i \in \mathbb{R}^{(S-1) \times C_2}$, which is fed into a lightweight MLP to produce the final prediction \hat{y}_i . The overall decoding strategy can be formally expressed as:

$$\tilde{W}_i = \text{TextDec}(W_i, [V_i^{(1)}, V_i^{(2,n)}]) \in \mathbb{R}^{(S-1) \times C_2}$$

where $[\cdot]$ denotes the concatenation operation, and TextDec refers to the image-guided text decoder.

3.2.5. Summary

Low-resolution images provide global visual representation, masked image modeling encourages learning of fine-grained local features from high-resolution sub-images. The text-guided image decoder enforces text-aware reconstruction, and

the image-guided text decoder enables the text modality to assimilate multi-scale visual cues. This symmetrical bidirectional fusion thus exploits non-verbal visual cues at both local and global representations while preserving effective use of verbal cues, yielding mutual guidance and semantic alignment between different modalities.

3.3. Loss Functions

3.3.1. Reconstruction Loss

We need to calculate error between predicted pixel values and real pixel values when utilizing masked image modeling. We minimize *mean square error* over in the pixel space between the masked image tokens in the high-resolution sub-images and the reconstructed tokens, and use it as the reconstruction loss to optimize fine-grained feature extraction capability of the image encoder:

$$\mathcal{L}_{\text{rec}} = \frac{1}{N} \sum_{i=1}^N \left(\frac{1}{\sum_n |\bar{M}_{i,n}|} \sum_n \sum_{p \in \bar{M}_{i,n}} \|X_{i,n}^p - \tilde{X}_{i,n}^p\|_2 \right) \quad (2)$$

where $X_{i,n}^p$ is the RGB pixel value of the high-resolution sub-images, and $\tilde{X}_{i,n}^p$ is the predicted pixel value. $|\bar{M}_{i,n}|$ denotes the number of masked tokens in the n -th sub-image of the i -th high-resolution sub-images, and $\|\cdot\|_2$ refers to the L_2 loss.

3.3.2. Image-Text Contrastive Loss

To facilitate the alignment of image and text modalities in a shared semantic space, we introduce an image-text contrastive loss. Given the normalized global visual representation v_i^{cls} from the low-resolution image and the global text representation w_i^{cls} , the loss is defined to align the image and text representation:

$$\mathcal{L}_{\text{itc}} = \frac{1}{2N} \left[\sum_{i=1}^N -\log \left(\frac{\exp(\langle v_i^{\text{cls}}, w_i^{\text{cls}} \rangle / \tau)}{\sum_{j=1}^N \exp(\langle v_i^{\text{cls}}, w_j^{\text{cls}} \rangle / \tau)} \right) \right] + \frac{1}{2N} \left[\sum_{i=1}^N -\log \left(\frac{\exp(\langle w_i^{\text{cls}}, v_i^{\text{cls}} \rangle / \tau)}{\sum_{j=1}^N \exp(\langle w_i^{\text{cls}}, v_j^{\text{cls}} \rangle / \tau)} \right) \right] \quad (3)$$

where $\langle \cdot, \cdot \rangle$ denotes the inner product, and τ is a temperature hyperparameter. This loss encourages matched image-text pairs to cluster together in the semantic space while pushing unmatched pairs apart, thereby enhancing cross-modal consistency.

3.3.3. Local-Global Semantic Similarity Loss

Although using high-resolution sub-images as input in masked image modeling helps extract fine-grained local features, it may also cause the reconstructed tokens to deviate from the global visual semantic information from low-resolution images, resulting in over rely local information. To enforce consistency between the reconstructed local features and the global visual representations, we perform learnable weighted aggregation on the sub-image-level global representation $\{z_{i,n}\}_{n=1}^4$ to

obtain:

$$\begin{aligned} e_{i,n} &= u^T \tanh(z_{i,n} W_z + b) \\ \alpha_{i,n} &= [\text{softmax}([e_{i,1}, \dots, e_{i,4}])]_n \\ P_{\text{agg},i} &= \text{MLP}\left(\sum_{n=1}^4 \alpha_{i,n} z_{i,n}\right) \end{aligned}$$

here, W_z , u , b are learnable parameters, and the MLP projects the aggregated feature into same semantic space as v_i^{cls} . After normalizing to all features, the similarity loss is computed as:

$$\mathcal{L}_{si} = \frac{1}{N} \sum_{i=1}^N \|v_i^{\text{cls}} - P_{\text{agg},i}\|_2^2 \quad (4)$$

This loss ensures that the reconstructed local pixel features from high-resolution sub-images remain consistent with the global image semantics from low-resolution images, achieving a balance between local and global features.

3.3.4. Cross-Modal Feature-Distribution Consistency Loss

There exists a conflict between the objectives of the contrastive loss (semantic-level) and the reconstruction loss (pixel-level). The former emphasizes cross-modal semantic alignment, while the latter focuses on pixel-level reconstruction quality without explicitly enforcing semantic consistency across modalities. To mitigate this, we constrain the semantic distribution consistency between the text to reconstructed image features and the text to low-resolution image features. Specifically, the similarity distribution between the aggregated reconstructed image feature $P_{\text{agg},i}$ and the global text representation w_i^{cls} is defined as:

$$S(P_{\text{agg},i}, w_i^{\text{cls}}) = \frac{\exp(\langle P_{\text{agg},i}, w_i^{\text{cls}} \rangle / \tau)}{\sum_{j=1}^N \exp(\langle P_{\text{agg},i}, w_j^{\text{cls}} \rangle / \tau)}$$

Similarly, the similarity distribution $S(v_i^{\text{cls}}, w_i^{\text{cls}})$ is defined for the low-resolution image feature and the global text representation. By minimizing the KL divergence between the two distributions and adding an entropy regularization term for robustness, we obtain the following loss:

$$\begin{aligned} \mathcal{L}_{dc} &= \frac{1}{N} \sum_{i=1}^N \text{KL}(S(P_{\text{agg},i}, w_i^{\text{cls}}), S(v_i^{\text{cls}}, w_i^{\text{cls}})) \\ &+ \frac{1}{N} \sum_{i=1}^N H(S(P_{\text{agg},i}, w_i^{\text{cls}})) \end{aligned} \quad (5)$$

where KL denotes the relative entropy loss function, H represents the entropy function.

3.3.5. Classification Loss

For downstream tasks, such as desire understanding, emotion recognition, and sentiment analysis, we use the standard cross-entropy loss:

$$\mathcal{L}_{cls} = \frac{1}{N} \sum_{i=1}^N \text{CrossEntropy}(y_i, \hat{y}_i) \quad (6)$$

where y is the ground-truth label and \hat{y}_i is the predicted label.

3.4. Two-stage Training Strategy

To balance semantic alignment with pixel-level reconstruction, we adopt a two-stage training strategy and selectively freeze or unfreeze model components in each stage to steer learning.

3.4.1. Pre-training Stage

The pre-training stage focuses on masked image modeling, giving priority to training the image encoder and the text-guided image decoder. In this stage, we freeze the image-guided text decoder and the MLP, and only update the text encoder, the image encoder, and the text-guided image decoder. This design allows us to extract fine-grained details from high-resolution sub-images while constraining modal consistency at the semantic level. As discussed in Section 3.3.3 and Section 3.3.4, we also consider the sub-image-level global visual representation of reconstructed image tokens and their cross-modal alignment. Therefore, the overall loss used in this stage is:

$$\mathcal{L}_p = \lambda_{rec} \mathcal{L}_{rec} + \lambda_{si} \mathcal{L}_{si} + \lambda_{dc} \mathcal{L}_{dc} + \lambda_{itc} \mathcal{L}_{itc} \quad (7)$$

where λ_{rec} , λ_{si} , λ_{dc} and λ_{itc} are hyperparameter weights that balance the contributions of each loss term.

3.4.2. Fine-tuning Stage

The fine-tuning stage targets downstream tasks such as desire understanding. Its goal is to train the image-guided text decoder to fully leverage both local and global features produced by the image encoder, and to use an MLP to map the fused multimodal representation to task-specific outputs. During fine-tuning we freeze the image encoder and text-guided image decoder, and train the text encoder, the image-guided text decoder, and the MLP. The overall loss for this stage is:

$$\mathcal{L}_f = \lambda_{cls} \mathcal{L}_{cls} + \lambda_{itc} \mathcal{L}_{itc} \quad (8)$$

where λ_{cls} and λ_{itc} are hyperparameter weights. Retaining the ITC term helps preserve cross-modal alignment stability during fine-tuning.

Table 1: Data statistics of MSED dataset

Task	Label	Train	Validation	Test
Sentiment Analysis	Positive	2,524	419	860
	Neutral	1,664	294	569
	Negative	1,939	308	613
Emotion Recognition	Happiness	2,524	419	860
	Sad	666	102	186
	Neutral	1,664	294	569
	Disgust	251	44	80
	Anger	523	78	172
	Fear	499	84	175
Desire Understanding	Vengeance	277	39	75
	Curiosity	634	118	213
	Social-contact	437	59	138
	Family	873	152	288
	Tranquility	245	39	87
	Romance	692	101	210
	None	2,969	507	1,031

4. Experiments

4.1. Experiment Setup

4.1.1. Dataset

To validate our method, we evaluate the model on the publicly available multimodal dataset MSED [39]. MSED is the first multimodal, multi-task dataset for sentiment analysis, emotion recognition, and desire understanding and contains 9,190 image-text pairs annotated in English. The samples are collected from social media platforms, including Twitter, Getty Image, and Flickr. The dataset defines three downstream tasks: sentiment analysis, emotion recognition, and desire understanding. Each multimodal sample is manually labeled with sentiment class (*positive, neutral, negative*), an emotion class (*happiness, sad, neutral, disgust, anger, and fear*), and a desire class (*family, romance, vengeance, curiosity, tranquility, social-contact, and none*). The data are split into train, validation, and test sets with ratios of 70%, 10%, and 20%, yielding 6,127 training instances, 1,021 validation instances, and 2,024 test instances. The detailed statistics of the MSED dataset are listed in Table 1.

4.1.2. Evaluation Metrics

All three downstream tasks are classification problems. We therefore report standard classification metrics: Precision (P), Recall (R), Macro-F1-score (F1), and Weighted Accuracy (Acc).

4.1.3. Training Details

All experiments run on NVIDIA V100 with CUDA 11.0 and PyTorch 2.1.2 [42]. In pre-training stage, we initialize the image encoder and the text encoder from CLIP [43] pre-training weights provided by OpenAI¹, and initialize the text-guided image decoder from pre-training weights² in [44]. We use the AdamW [45] optimizer. The initial learning rates for the image encoder, the text encoder, and text-guided image decoder are set to $5e-6$, $5e-5$, and $1e-4$, respectively. Weight decay is 0.01. The learning rate follows a cosine decay schedule with a 15% warmup period. We train for 50 epochs with batch size 64. Loss weights are set to $\lambda_{rec} = 1$, $\lambda_{si} = 0.5$, $\lambda_{dc} = 0.025$, and $\lambda_{itc} = 0.5$. The masking ratio m is 0.75 during pre-training.

During fine-tuning stage, we keep the overall setup and fine-tune the pretrained model separately for desire understanding, emotion recognition, and sentiment analysis. Specifically, the initial learning rates for the text encoder, image-guided text decoder, and MLP are $1e-4$, $2e-4$, and $1e-4$, respectively, with a 10% warmup. Fine-tuning uses batch size 64 for 50 epochs. Loss weights are $\lambda_{cls} = 1$ and $\lambda_{itc} = 0.4$. In fine-tuning, images are no longer masked, we feed the full low-resolution image along with high-resolution sub-images. The masking ratio m is thus set to 0.00.

Table 2: Comparison between SyDES and different modality baseline models on the MSED dataset

Task	Method	Modality	P	R	F1
Sentiment Analysis	BERTweet	Text	82.25	83.62	82.49
	ResNet	Image	70.85	70.61	70.64
	SyDES-B	Multimodal	89.09	85.58	86.50
	SyDES	Multimodal	89.28	89.13	89.19
Emotion Recognition	BERTweet	Text	80.99	77.15	78.34
	ResNet	Image	58.74	54.67	56.40
	SyDES-B	Multimodal	81.04	80.66	80.80
	SyDES	Multimodal	84.92	84.81	84.74
Desire Understanding	BERTweet	Text	77.11	81.19	78.86
	ResNet	Image	49.97	49.35	49.20
	SyDES-B	Multimodal	80.77	67.43	72.27
	SyDES	Multimodal	84.09	84.07	84.02

4.1.4. Baseline

To facilitate subsequent ablation analysis and comparison, we use the SyDES architecture trained directly with classification loss without pre-training stage. We denote this variant as **SyDES-B** (the SyDES baseline).

4.2. Comparison with different modality baseline models

We compared different modality baseline models on three downstream tasks, including desire understanding, emotion recognition, and sentiment analysis, to evaluate the effectiveness of our proposed SyDES. For the textual modality, we employed **BERTweet** [46] model as the baseline modal since text data are annotated from social media platforms. For the image modality, we used the classic backbone network **ResNet** [47]. The multimodal baseline model, SyDES-B, was included to demonstrate the advantage of multimodal fusion. We also present the results of our proposed SyDES method.

The experiment results for different modality baseline models are shown in Table 2. In sentiment analysis, BERTweet achieved an F1-score of 82.49%, ResNet 70.64%, SyDES-B 86.50%, and SyDES 89.19%. For emotion recognition, the F1-scores were 78.34% for BERTweet, 56.40% for ResNet, 80.80% for SyDES-B, and 84.74% for SyDES. In desire understanding, BERTweet scored 78.86%, ResNet 49.20%, SyDES-B 72.27%, and SyDES reached 84.02%.

Analysis of these results leads to three main conclusions: (1) Multimodal models consistently outperform unimodal models across mostly tasks. For instance, in emotion recognition, SyDES-B improved the F1-score by 3.14% gains over BERTweet, indicating the benefit of leveraging multiple modalities in sentiment-related tasks. (2) The unimodal image model (e.g., ResNet) consistently underperformed compared to the unimodal text model (e.g., BERTweet), suggesting limitations in capturing fine-grained visual semantics and underutilization of non-verbal cues. This further highlights the necessity of our proposed method. (3) Our proposed SyDES consistently surpassed SyDES-B in all tasks, validating the effectiveness of the non-verbal cues mining mechanism introduced during pre-training.

4.3. Comparison with state-of-the-art methods

We propose SyDES, a symmetrical bidirectional multimodal learning framework that leverages masked image modeling

¹<https://github.com/openai/CLIP>

²https://huggingface.co/laion/mscoco_finetuned_CoCa-ViT-L-14-laion2B-s13B-b90k

Table 3: Comparison of SyDES and other SOTA methods on the MSED dataset

Method	Desire Understanding				Emotion Recognition				Sentiment Analysis			
	P	R	F1	Acc	P	R	F1	Acc	P	R	F1	Acc
DCNN+AlexNet [39]	59.42	52.02	52.35	-	49.56	42.77	43.76	-	71.02	70.09	70.31	-
DCNN+ResNet [39]	56.34	50.64	52.89	-	62.93	59.12	60.48	-	74.73	74.73	74.64	-
BiLSTM+AlexNet [39]	67.80	68.00	67.67	-	71.17	70.70	70.89	-	78.73	79.22	78.89	-
BERT+AlexNet [39]	80.84	75.50	77.17	-	78.06	78.19	78.10	-	83.22	83.11	83.16	-
Multimodal Transformer [39]	81.92	80.20	80.92	-	81.62	81.61	81.53	-	83.56	83.45	83.50	-
M3GAT [30]	-	-	-	-	82.53	81.51	81.97	-	84.66	85.15	84.85	-
MMTF-DES [40]	84.23	<u>82.01</u>	<u>83.11</u>	<u>86.97</u>	<u>84.39</u>	<u>84.64</u>	<u>84.26</u>	<u>84.13</u>	<u>88.27</u>	<u>88.68</u>	<u>88.44</u>	<u>88.44</u>
SyDES (Ours)	<u>84.09</u>	84.07	84.02	88.32	84.92	84.81	84.74	85.96	89.28	89.13	89.19	89.37
%Gains	-0.20	+2.50	+1.10	+1.60	+0.60	+0.20	+0.60	+2.20	+1.10	+0.50	+0.90	+1.10

to effectively integrate textual features with both local and global visual features for desire understanding. To evaluate SyDES and validate the effectiveness of non-verbal cues mining mechanism, we conducted experiments on the MSED dataset, which comprises three sub-tasks, including desire understanding, emotion recognition, and sentiment analysis.

The comparative performance of our proposed SyDES on test data against other SOTA methods across all tasks is presented in Table 3. The results indicate that SyDES achieves competitive performance across all three tasks. In terms of the primary metric F1-score, our proposed SyDES achieves 84.02% in desire understanding, 84.74% in emotion recognition, and 89.19% in sentiment analysis, surpassing the previous best model, MMTF-DES [40], by 1.1%, 0.6%, and 0.9% gains, respectively. It is worth noting that MMTF-DES relies on integrating multiple multimodal Transformer encoders (e.g., ViLT and VAULT), which entails considerably higher training costs. In contrast, SyDES extracts non-verbal cues from images effectively while maintaining lower computational overhead. The experimental results validate this trade-off: the improvement on the desire understanding task, which depends more heavily on non-verbal cues, is particularly pronounced in terms of the F1-score.

We further observe that sentiment analysis generally yields higher performance than for the emotion recognition and desire understanding tasks. A possible reason for this difference in performance may be attributed to the nature of the three tasks. Sentiment analysis aim to identify the overall emotion or opinion expressed in an image-text pair. In contrast, desire understanding and emotion recognition require fine-grained detection of specific signals such as a person’s gestures or facial expressions that are inherently embedded in images. For example, there exists the exaggerated motion and frightened expression of the man in Figure 1 (b). These subtle cues are inherently more challenging to capture. Therefore, sentiment analysis may be an easier and more straightforward task for model, while desire understanding and emotion recognition may be more complicated and nuanced. Our proposed SyDES enhances local detail extraction, resulting in particularly notable gains in desire understanding, but its performance remains slightly below that of sentiment analysis. This suggests there is still room for improvement and underscores the need for further research into

desire understanding and emotion recognition.

4.4. Ablation Studies

4.4.1. Loss Functions

We adopt a two-stage training strategy to facilitate cross-modal fusion between textual features and both local and global visual features. As summarized in Table 4, we systematically evaluate the impact of different loss combinations on the three sub-tasks. The first row corresponds to the model fin-tuned directly without pre-training stage (i.e., SyDES-B as described in Section 4.1.4). During pre-training, four loss functions are used, including \mathcal{L}_{rec} , \mathcal{L}_{si} , \mathcal{L}_{dc} , and \mathcal{L}_{itc} . Results show that using only \mathcal{L}_{rec} for masked image modeling leads to performance even worse than SyDES-B. This indicates that reconstructing high-resolution sub-images alone may introduce a semantic mismatch with the low-resolution image due to inadequate modal alignment, resulting in modal inconsistency that harms fine-tuning. Gradually incorporating \mathcal{L}_{itc} , \mathcal{L}_{si} , and \mathcal{L}_{dc} consistently improves performance across all tasks. For example, in desire understanding, the F1-score increases to 81.44% with \mathcal{L}_{itc} , to 82.24% with \mathcal{L}_{si} , and finally to 84.02% with \mathcal{L}_{dc} . This suggests that cross-modal alignment and semantic/consistency constraints are critical to bridging the gap between reconstructed sub-images and the global image semantics.

During fine-tuning, two loss functions are used, including \mathcal{L}_{itc} and \mathcal{L}_{cls} . We observe that that \mathcal{L}_{itc} is important to preserve pre-training gains. Removing \mathcal{L}_{itc} during fine-tuning causes the F1-scores to drop from 84.02%, 84.74%, and 89.19% to 77.09%, 83.21%, and 86.16%, respectively. In conclusion, using all proposed loss functions yields the best performance across desire understanding, emotion recognition, and sentiment analysis, confirming the complementary effects of the loss terms.

4.4.2. Ratio of Masked Tokens

As shown in Table 5, we investigate the impact by setting different ratios of masked tokens. Specifically, 0.25, 0.50, 0.75, and 0.90 are tested. Experimental results demonstrate that a masking ratio of 75% yields the best average performance across most tasks. Although a ratio of 25% achieves slightly better results in emotion recognition, the 75% ratio is overall

Table 4: Ablation study on the loss functions used in the two training stages

Pre-training				Fine-tuning		Desire Understanding				Emotion Recognition				Sentiment Analysis			
\mathcal{L}_{rec}	\mathcal{L}_{itc}	\mathcal{L}_{si}	\mathcal{L}_{dc}	\mathcal{L}_{itc}	\mathcal{L}_{cls}	P	R	F1	Acc	P	R	F1	Acc	P	R	F1	Acc
×	×	×	×	×	✓	80.77	67.43	72.27	80.51	81.04	80.66	80.80	82.61	89.09	85.58	86.50	87.12
✓	×	×	×	✓	✓	76.17	72.56	74.12	81.15	76.78	75.13	75.82	77.62	80.57	81.19	80.79	80.80
✓	✓	×	×	✓	✓	81.43	81.77	81.44	86.19	84.85	84.95	84.66	85.21	89.26	88.80	88.99	89.18
✓	✓	✓	×	✓	✓	82.28	82.33	82.24	86.78	84.17	81.91	82.88	84.53	87.45	87.66	87.55	87.71
✓	✓	✓	✓	×	✓	78.55	75.89	77.09	83.74	84.85	81.75	83.21	84.43	86.46	85.93	86.16	86.44
✓	✓	✓	✓	✓	✓	84.09	84.07	84.02	88.32	84.92	84.81	84.74	85.96	89.28	89.13	89.19	89.37

Table 5: Ablation study on the ratio of masked tokens

Ratio of Masked Tokens		Desire Understanding				Emotion Recognition				Sentiment Analysis			
		P	R	F1	Acc	P	R	F1	Acc	P	R	F1	Acc
0.25		83.13	81.80	82.23	86.82	85.94	85.30	85.55	85.94	88.90	89.05	88.87	88.83
0.50		81.87	81.69	81.69	86.48	84.36	84.35	84.19	85.06	87.64	88.18	87.88	88.06
0.75		84.09	84.07	84.02	88.32	84.92	84.81	84.74	85.96	89.28	89.13	89.19	89.37
0.90		81.31	82.82	82.02	86.48	84.32	83.31	83.78	85.41	88.54	87.93	88.17	88.39










Sentiment Analysis	 Brother and sister exploring with flashlight. Class Label: Negative SyDES-B: × (0.4441) SyDES: ✓ (0.9621)	 Cute little girl learning on the lawn. Class Label: Positive SyDES-B: × (0.1406) SyDES: ✓ (0.9878)	 Young man distracted while on video call from his home during lockdown. Class Label: Neutral SyDES-B: × (0.1638) SyDES: ✓ (0.9999)
	 Smiling couple hiking together. Class Label: Neutral SyDES-B: × (0.0084) SyDES: ✓ (0.7779)	 Congressman (Frank Lautenberg) refuses to take the non-partisan oath while colleagues William Stepien offer him. Lafayette was against the temperance movement and prohibition of the 1920s. Class Label: Disgust SyDES-B: × (0.1801) SyDES: ✓ (0.9998)	 Mother and daughters watching television, holding breaths. Class Label: Fear SyDES-B: × (0.0291) SyDES: ✓ (0.6755)
	 Woman wearing a tiger mask spring, kneeling on her husband, bond with handcuffs to the bed in their bedroom. Couple Concept Portrait. Class Label: Vengeance SyDES-B: × (0.3354) SyDES: ✓ (0.9589)	 Shoot of office staff jumping. Class Label: Social-contact SyDES-B: × (0.2841) SyDES: ✓ (0.8099)	 Anatolia, Salzkommergut, Cheering couple reaching mountain summit. Class Label: Romance SyDES-B: × (0.1091) SyDES: ✓ (0.7188)

Figure 3: Performance analysis of our proposed SyDES on desire understanding, emotion recognition, and sentiment analysis tasks. A × indicates correct classification and a ✓ represents misclassification.

more suitable considering its substantially lower computational cost while maintain competitive performance.

4.4.3. Performance Analysis

To better understand the advantage of our proposed SyDES, we selected representative examples from the MSSED dataset across three sub-tasks. These examples are misclassified by SyDES-B but correctly classified by SyDES. As illustrated in Figure 3, we compare the predictions of SyDES-B and our proposed SyDES, including example stimuli, ground-truth labels, and predicted probabilities. Across all three tasks, our proposed SyDES produces correct predictions with high confidence. For instance, in Example 1 of the sentiment analysis task, the image caption is “*Brother and sister exploring with flashlight.*”, it provides limited information. But our proposed SyDES achieved a high confidence score of 96.21% by effectively leveraging visual cues. This evidence indicates that, compared with models that rely mainly on transfer learning with pre-trained weights (e.g., SyDES-B), the non-verbal cues mining and symmetric bidirectional multimodal learning mechanism introduced in the

pre-training stage of our proposed SyDES are effective. It substantially improves robustness and accuracy, especially when textual information is limited.

4.5. Visualization

4.5.1. Cross-Modal Attention Heatmap Analysis

To intuitively illustrate the perception ability of our proposed SyDES toward textual and image modalities, we visualized the attention localization map for the last layer in the image encoder, and compared them with those of SyDES-B. As depicted in Figure 4, our proposed SyDES focuses more accurately on fine-grained visual regions corresponding to informative words in the text. For example, in the case of Image 1, SyDES shows concentrated attention on regions related to “*boy*” and “*bike*”, whereas SyDES-B neglects these essential details. Similarity, in the case of Image 3, SyDES-B perceives the concept of “*family*” vaguely, while our proposed SyDES clearly identifies the five-person “*family*” and the “*beach*” scene. This improved perception can be attributed to two mechanisms: (1) the masked image modeling on high-resolution sub-images, which enhances local detail sensitivity; (2) the text-guided cross-modal reconstruction, which strengthens cross-modal semantic alignment. These results further indicate that our proposed SyDES effectively exploits non-verbal visual cues.

4.5.2. Reconstructed Image Visualization

We reconstructed and stitched the high-resolution sub-images, and visualized the masked image patches to inspect the practical effect in Figure 5. Each sample consists of the original image, the randomly masked image, and the reconstructed image by the text-guided image decoder. The results show that, even with complex image content (e.g., *people*, *gesture*, *lighting*, and *natural scenes* in the example 1), our proposed SyDES can reconstruct contextual content reasonably well, owing to masked image modeling using high-resolution sub-images and

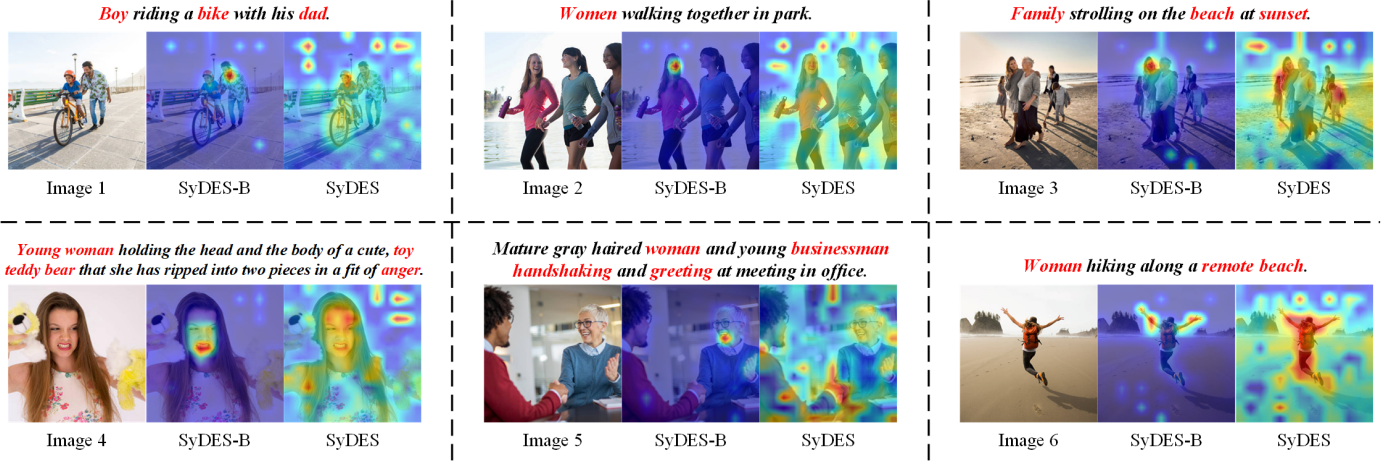


Figure 4: Qualitative analysis of attention localization map in our proposed SyDES. We visualize the attention localization map from the last layer in the image encoder, reflecting the model’s cross-modal perception of text.

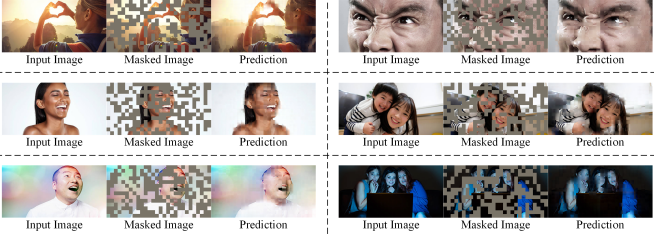


Figure 5: Visualization of reconstructed images using our proposed SyDES.

text-guided decoding. However, we also observe limitations in reconstructing fine facial details. This is likely because faces occupy a small fraction of the overall image and contain intricate features (e.g., *eyes*, *nose*, *mouth*) that require more fine-grained reconstruction methods. The local multi-scale reconstruction proposed in [48] appears promising and warrants further exploration to address these limitations.

5. Discussion

Although we thoroughly explore non-verbal cues in images through a masked image modeling and our proposed method demonstrated effectiveness on the MSED dataset, several limitations remain:

- (1) Capturing fine-grained local features is still insufficient. As shown in Section 4.5.2, reconstructions of small but semantically important region such as faces are limited, indicating that there is still room for improvement in perceiving and reconstructing fine-grained regions.
- (2) The exploitation of textual information could be further enhanced. Textual descriptions often obtain abundant aspect-level expressions (e.g., opinion words). Effectively leveraging such terms, integrating and aligning them with visual information represents a promising direction for future research.

- (3) The current method focuses only on image-text pairs. Real-world multimodal data involve additional modalities (e.g., video and audio), which provide richer non-verbal cues. Extending our method to incorporate more modalities while balancing computational cost and performance constitutes an important direction for further investigation.

6. Conclusion

To address the under-exploration of desire understanding and of non-verbal cues in multimodal sentiment analysis, we propose a symmetric bidirectional multimodal learning framework for desire, emotion, and sentiment recognition. The framework employs a masked image modeling to boosting extract fine-grained local features from high-resolution sub-images and capturing global visual representations from low-resolution images. More, we introduce a text-guided image decoder and an image-guided text decoder so that facilitate semantic alignment and modal fusion from local and global features during decoding, thereby enhancing the discriminative power of multimodal representations. Extensive experiments on the MSED dataset across three sub-tasks, demonstrate the effectiveness of our proposed method. We expect this work to offer insights for multimodal desire understanding and to inspire further research in this field.

Declaration of competing interest

The authors declare that they have no known competing financial interests or personal relationships that could have appeared to influence the work reported in this paper.

Data availability

The MSED dataset [39] used in this paper are publicly available datasets. We respect valuable and creative works in the area of sarcasm detection and other related research.

Acknowledgments

This work is supported by the National Natural Science Foundation of China (Grant No. 62272188), the Fundamental Research Funds for the Central Universities (Grant No. 2662021JC008), and the 2023 Independent Science and Technology Innovation Fund Project of Huazhong Agricultural University (Grant No. 2662023XXPY005).

References

- [1] Y. Kim, [Convolutional neural networks for sentence classification](https://api.semanticscholar.org/CorpusID:9672033), in: Conference on Empirical Methods in Natural Language Processing, 2014.
URL <https://api.semanticscholar.org/CorpusID:9672033>
- [2] Z. Yang, D. Yang, C. Dyer, X. He, A. Smola, E. H. Hovy, [Hierarchical attention networks for document classification](https://api.semanticscholar.org/CorpusID:6857205), in: North American Chapter of the Association for Computational Linguistics, 2016.
URL <https://api.semanticscholar.org/CorpusID:6857205>
- [3] G. Liu, J. Guo, [Bidirectional lstm with attention mechanism and convolutional layer for text classification](https://api.semanticscholar.org/CorpusID:127325665), *Neurocomputing* 337 (2019) 325–338.
URL <https://api.semanticscholar.org/CorpusID:127325665>
- [4] N. Xu, W. Mao, [Multisentinet: A deep semantic network for multimodal sentiment analysis](https://api.semanticscholar.org/CorpusID:29030535), *Proceedings of the 2017 ACM on Conference on Information and Knowledge Management* (2017).
URL <https://api.semanticscholar.org/CorpusID:29030535>
- [5] X. Yang, S. Feng, D. Wang, Y. Zhang, [Image-text multimodal emotion classification via multi-view attentional network](https://api.semanticscholar.org/CorpusID:229272644), *IEEE Transactions on Multimedia* 23 (2020) 4014–4026.
URL <https://api.semanticscholar.org/CorpusID:229272644>
- [6] Z. Liu, Y. Shen, V. B. Lakshminarasimhan, P. P. Liang, A. Zadeh, L. philippe Morency, [Efficient low-rank multimodal fusion with modality-specific factors](https://api.semanticscholar.org/CorpusID:44131945), *ArXiv abs/1806.00064* (2018).
URL <https://api.semanticscholar.org/CorpusID:44131945>
- [7] P. Portner, A. Rubinstein, [Desire, belief, and semantic composition: variation in mood selection with desire predicates](https://api.semanticscholar.org/CorpusID:226352313), *Natural Language Semantics* 28 (2020) 343 – 393.
URL <https://api.semanticscholar.org/CorpusID:226352313>
- [8] W. Hofmann, L. F. Nordgren, *The psychology of desire*, Guilford Publications, 2015.
- [9] X. Yang, S. Feng, Y. Zhang, D. Wang, [Multimodal sentiment detection based on multi-channel graph neural networks](https://api.semanticscholar.org/CorpusID:236460184), in: Annual Meeting of the Association for Computational Linguistics, 2021.
URL <https://api.semanticscholar.org/CorpusID:236460184>
- [10] T. Zhu, L. Li, J. Yang, S. Zhao, X. Xiao, [Multimodal emotion classification with multi-level semantic reasoning network](https://api.semanticscholar.org/CorpusID:253313650), *IEEE Transactions on Multimedia* 25 (2023) 6868–6880.
URL <https://api.semanticscholar.org/CorpusID:253313650>
- [11] B. Pang, L. Lee, S. Vaithyanathan, Thumbs up? sentiment classification using machine learning techniques, *arXiv preprint cs/0205070* (2002).
- [12] K. S. Tai, R. Socher, C. D. Manning, [Improved semantic representations from tree-structured long short-term memory networks](https://api.semanticscholar.org/CorpusID:3033526), *ArXiv abs/1503.00075* (2015).
URL <https://api.semanticscholar.org/CorpusID:3033526>
- [13] M. Singh, A. K. Jakhar, S. Pandey, [Sentiment analysis on the impact of coronavirus in social life using the bert model](https://api.semanticscholar.org/CorpusID:232293517), *Social Network Analysis and Mining* 11 (2021).
URL <https://api.semanticscholar.org/CorpusID:232293517>
- [14] M. Taboada, J. Brooke, M. Tofiloski, K. Voll, M. Stede, Lexicon-based methods for sentiment analysis, *Computational linguistics* 37 (2) (2011) 267–307.
- [15] P. Gamallo, M. Garcia, Citius: A naive-bayes strategy for sentiment analysis on english tweets, in: *Proceedings of the 8th international Workshop on Semantic Evaluation (SemEval 2014)*, 2014, pp. 171–175.
- [16] Y. Wang, M. Huang, X. Zhu, L. Zhao, [Attention-based lstm for aspect-level sentiment classification](https://api.semanticscholar.org/CorpusID:18993998), in: Conference on Empirical Methods in Natural Language Processing, 2016.
URL <https://api.semanticscholar.org/CorpusID:18993998>
- [17] Q. You, J. Luo, H. Jin, J. Yang, [Cross-modality consistent regression for joint visual-textual sentiment analysis of social multimedia](https://api.semanticscholar.org/CorpusID:7928793), *Proceedings of the Ninth ACM International Conference on Web Search and Data Mining* (2016).
URL <https://api.semanticscholar.org/CorpusID:7928793>
- [18] N. Xu, W. Mao, G. Chen, [A co-memory network for multimodal sentiment analysis](https://api.semanticscholar.org/CorpusID:195351351), *The 41st International ACM SIGIR Conference on Research & Development in Information Retrieval* (2018).
URL <https://api.semanticscholar.org/CorpusID:195351351>

- [19] F. Huang, K. Wei, J. Weng, Z. Li, [Attention-based modality-gated networks for image-text sentiment analysis](https://api.semanticscholar.org/CorpusID:218517893), ACM Transactions on Multimedia Computing, Communications, and Applications (TOMM) 16 (2020) 1 – 19.
URL <https://api.semanticscholar.org/CorpusID:218517893>
- [20] A. Hu, S. Flaxman, [Multimodal sentiment analysis to explore the structure of emotions](https://api.semanticscholar.org/CorpusID:44075392), Proceedings of the 24th ACM SIGKDD International Conference on Knowledge Discovery & Data Mining (2018).
URL <https://api.semanticscholar.org/CorpusID:44075392>
- [21] Z. Li, B. Xu, C. Zhu, T. Zhao, [Clmlf: A contrastive learning and multi-layer fusion method for multimodal sentiment detection](https://api.semanticscholar.org/CorpusID:248119031), ArXiv abs/2204.05515 (2022).
URL <https://api.semanticscholar.org/CorpusID:248119031>
- [22] H. Ranganathan, S. Chakraborty, S. Panchanathan, [Multimodal emotion recognition using deep learning architectures](https://api.semanticscholar.org/CorpusID:6182290), 2016 IEEE Winter Conference on Applications of Computer Vision (WACV) (2016) 1–9.
URL <https://api.semanticscholar.org/CorpusID:6182290>
- [23] Y. Zhang, C. Cheng, Y. Zhang, [Multimodal emotion recognition based on manifold learning and convolution neural network](https://api.semanticscholar.org/CorpusID:248252616), Multimedia Tools and Applications 81 (2022) 33253 – 33268.
URL <https://api.semanticscholar.org/CorpusID:248252616>
- [24] H.-D. Le, G. Lee, S. hyung Kim, S. won Kim, H.-J. Yang, [Multi-label multimodal emotion recognition with transformer-based fusion and emotion-level representation learning](https://api.semanticscholar.org/CorpusID:256944875), IEEE Access 11 (2023) 14742–14751.
URL <https://api.semanticscholar.org/CorpusID:256944875>
- [25] W. Guo, Y. Zhang, X. Cai, L. Meng, J. Yang, X. Yuan, [Ld-man: Layout-driven multimodal attention network for online news sentiment recognition](https://api.semanticscholar.org/CorpusID:226742001), IEEE Transactions on Multimedia 23 (2021) 1785–1798.
URL <https://api.semanticscholar.org/CorpusID:226742001>
- [26] S. Nemati, R. Rohani, M. E. Basiri, M. Abdar, N. Y. Yen, V. Makarenkov, [A hybrid latent space data fusion method for multimodal emotion recognition](https://api.semanticscholar.org/CorpusID:209320752), IEEE Access 7 (2019) 172948–172964.
URL <https://api.semanticscholar.org/CorpusID:209320752>
- [27] N. Xu, [Analyzing multimodal public sentiment based on hierarchical semantic attentional network](https://api.semanticscholar.org/CorpusID:20067030), 2017 IEEE International Conference on Intelligence and Security Informatics (ISI) (2017) 152–154.
URL <https://api.semanticscholar.org/CorpusID:20067030>
- [28] F. Scarselli, M. Gori, A. C. Tsoi, M. Hagenbuchner, G. Monfardini, [The graph neural network model](https://api.semanticscholar.org/CorpusID:206756462), IEEE Transactions on Neural Networks 20 (2009) 61–80.
URL <https://api.semanticscholar.org/CorpusID:206756462>
- [29] X. Liu, W. Liu, M. Zhang, J. Chen, L. Gao, C. C. Yan, T. Mei, [Social relation recognition from videos via multi-scale spatial-temporal reasoning](https://api.semanticscholar.org/CorpusID:198118474), 2019 IEEE/CVF Conference on Computer Vision and Pattern Recognition (CVPR) (2019) 3561–3569.
URL <https://api.semanticscholar.org/CorpusID:198118474>
- [30] Y. Zhang, A. Jia, B. Wang, P. Zhang, D. Zhao, P. Li, Y. Hou, X. Jin, D. Song, J. Qin, [M3gat: A multi-modal, multi-task interactive graph attention network for conversational sentiment analysis and emotion recognition](https://api.semanticscholar.org/CorpusID:258788073), ACM Transactions on Information Systems 42 (2023) 1 – 32.
URL <https://api.semanticscholar.org/CorpusID:258788073>
- [31] W. Wang, L. Ding, L. Shen, Y. Luo, H. Hu, D. Tao, [Wisdom: Improving multimodal sentiment analysis by fusing contextual world knowledge](https://api.semanticscholar.org/CorpusID:266977237), Proceedings of the 32nd ACM International Conference on Multimedia (2024).
URL <https://api.semanticscholar.org/CorpusID:266977237>
- [32] K. He, X. Chen, S. Xie, Y. Li, P. Doll’ar, R. B. Girshick, [Masked autoencoders are scalable vision learners](https://api.semanticscholar.org/CorpusID:243985980), 2022 IEEE/CVF Conference on Computer Vision and Pattern Recognition (CVPR) (2021) 15979–15988.
URL <https://api.semanticscholar.org/CorpusID:243985980>
- [33] A. Lim, T. Ogata, H. G. Okuno, [The desire model: Cross-modal emotion analysis and expression for robots](https://api.semanticscholar.org/CorpusID:20067030), Information Processing Society of Japan 5 (4) (2012).
- [34] S. Cacioppo, F. Bianchi-Demicheli, C. Frum, J. G. Pfaus, J. W. Lewis, [The common neural bases between sexual desire and love: a multilevel kernel density fmri analysis](https://api.semanticscholar.org/CorpusID:20067030), The journal of sexual medicine 9 (4) (2012) 1048–1054.
- [35] N. S. Schutte, J. M. Malouff, [A meta-analysis of the relationship between curiosity and creativity](https://api.semanticscholar.org/CorpusID:199157255), The Journal of Creative Behavior (2019).
URL <https://api.semanticscholar.org/CorpusID:199157255>
- [36] S. Hoppe, T. Loetscher, S. Morey, A. Bulling, [Recognition of curiosity using eye movement analysis](https://api.semanticscholar.org/CorpusID:20067030), Adjunct Proceedings of the 2015 ACM International Joint Conference on Pervasive and Ubiquitous Computing and

- Proceedings of the 2015 ACM International Symposium on Wearable Computers (2015).
URL <https://api.semanticscholar.org/CorpusID:15967389>
- [37] Ö. Yavuz, A. Karahoca, D. Karahoca, [A data mining approach for desire and intention to participate in virtual communities](#), International Journal of Electrical and Computer Engineering (IJECE) (2019).
URL <https://api.semanticscholar.org/CorpusID:208980057>
- [38] D. S. Chauhan, S. Dhanush, A. Ekbal, P. Bhattacharyya, All-in-one: A deep attentive multi-task learning framework for humour, sarcasm, offensive, motivation, and sentiment on memes, in: Proceedings of the 1st conference of the Asia-Pacific chapter of the association for computational linguistics and the 10th international joint conference on natural language processing, 2020, pp. 281–290.
- [39] A. Jia, Y. He, Y. Zhang, S. Uprety, D. Song, C. Lioma, [Beyond emotion: A multi-modal dataset for human desire understanding](#), in: North American Chapter of the Association for Computational Linguistics, 2022.
URL <https://api.semanticscholar.org/CorpusID:250391079>
- [40] A. Aziz, N. K. Chowdhury, M. A. Kabir, A. N. Chy, M. J. Siddique, [Mmtf-des: A fusion of multimodal transformer models for desire, emotion, and sentiment analysis of social media data](#), Neurocomputing 623 (2025) 129376.
URL <https://api.semanticscholar.org/CorpusID:275561806>
- [41] A. Dosovitskiy, L. Beyer, A. Kolesnikov, D. Weissenborn, X. Zhai, T. Unterthiner, M. Dehghani, M. Minderer, G. Heigold, S. Gelly, J. Uszkoreit, N. Houlsby, [An image is worth 16x16 words: Transformers for image recognition at scale](#), ArXiv abs/2010.11929 (2020).
URL <https://api.semanticscholar.org/CorpusID:225039882>
- [42] A. Paszke, S. Gross, F. Massa, A. Lerer, J. Bradbury, G. Chanan, T. Killeen, Z. Lin, N. Gimelshein, L. Antiga, A. Desmaison, A. Köpf, E. Yang, Z. DeVito, M. Raison, A. Tejani, S. Chilamkurthy, B. Steiner, L. Fang, J. Bai, S. Chintala, [Pytorch: An imperative style, high-performance deep learning library](#), ArXiv abs/1912.01703 (2019).
URL <https://api.semanticscholar.org/CorpusID:202786778>
- [43] A. Radford, J. W. Kim, C. Hallacy, A. Ramesh, G. Goh, S. Agarwal, G. Sastry, A. Askell, P. Mishkin, J. Clark, G. Krueger, I. Sutskever, [Learning transferable visual models from natural language supervision](#), in: International Conference on Machine Learning, 2021.
URL <https://api.semanticscholar.org/CorpusID:231591445>
- [44] G. Ilharco, M. Wortsman, R. Wightman, C. Gordon, N. Carlini, R. Taori, A. Dave, V. Shankar, H. Namkoong, J. Miller, H. Hajishirzi, A. Farhadi, L. Schmidt, [Openclip](#), if you use this software, please cite it as below. (Jul. 2021).
[doi:10.5281/zenodo.5143773](https://doi.org/10.5281/zenodo.5143773).
URL <https://doi.org/10.5281/zenodo.5143773>
- [45] I. Loshchilov, F. Hutter, [Decoupled weight decay regularization](#), in: International Conference on Learning Representations, 2017.
URL <https://api.semanticscholar.org/CorpusID:53592270>
- [46] D. Q. Nguyen, T. Vu, A. G.-T. Nguyen, [Bertweet: A pre-trained language model for english tweets](#), in: Conference on Empirical Methods in Natural Language Processing, 2020.
URL <https://api.semanticscholar.org/CorpusID:218719869>
- [47] K. He, X. Zhang, S. Ren, J. Sun, [Deep residual learning for image recognition](#), 2016 IEEE Conference on Computer Vision and Pattern Recognition (CVPR) (2015) 770–778.
URL <https://api.semanticscholar.org/CorpusID:206594692>
- [48] H. Wang, Y. Tang, Y. Wang, J. Guo, Z. Deng, K. Han, [Masked image modeling with local multi-scale reconstruction](#), 2023 IEEE/CVF Conference on Computer Vision and Pattern Recognition (CVPR) (2023) 2122–2131.
URL <https://api.semanticscholar.org/CorpusID:257427476>